Interfacial engineering of solution-processed Ni nanochain-SiOx (x

Xiaobai Yu, Xiaoxin Wang, Qinglin Zhang, and Jifeng Liu

Citation: Journal of Applied Physics **119**, 135301 (2016); doi: 10.1063/1.4945035
View online: http://dx.doi.org/10.1063/1.4945035
View Table of Contents: http://scitation.aip.org/content/aip/journal/jap/119/13?ver=pdfcov
Published by the AIP Publishing

Interfacial engineering of solution-processed Ni nanochain-SiO_x ($x < 2$) cermets towards thermodynamically stable, anti-oxidation solar selective absorbers

Xiaobai Yu,[1] Xiaoxin Wang,[1] Qinglin Zhang,[2] and Jifeng Liu[1,a)]
[1]*Thayer School of Engineering, Dartmouth College, 14 Engineering Drive, Hanover, New Hampshire 03755, USA*
[2]*Department of Chemical and Materials Engineering, University of Kentucky, 177 F. Paul Anderson Tower, Lexington, Kentucky 40506, USA*

(Received 23 October 2015; accepted 18 March 2016; published online 1 April 2016)

Cermet solar thermal selective absorber coatings are an important component of high-efficiency concentrated solar power (CSP) receivers. The oxidation of the metal nanoparticles in cermet solar absorbers is a great challenge for vacuum-free operation. Recently, we have demonstrated that oxidation is kinetically retarded in solution processed, high-optical-performance Ni nanochain-SiO_x cermet system compared to conventional Ni-Al_2O_3 system when annealed in air at 450–600 °C for several hours. However, for long-term, high-temperature applications in CSP systems, *thermodynamically* stable antioxidation behavior is highly desirable, which requires new mechanisms beyond kinetically reducing the oxidation rate. Towards this goal, in this paper, we demonstrate that pre-operation annealing of Ni nanochain-SiO_x cermets at 900 °C in N_2 forms the thermodynamically stable orthorhombic phase of NiSi at the Ni/SiO_x interfaces, leading to self-terminated oxidation at 550 °C in air due to this interfacial engineering. In contrast, pre-operation annealing at a lower temperature of 750 °C in N_2 (as conducted in our previous work) cannot achieve interfacial NiSi formation directly, and further annealing in air at 450–600 °C for >4 h only leads to the formation of the less stable (metastable) hexagonal phase of NiSi. Therefore, the high-temperature pre-operation annealing is critical to form the desirable orthorhombic phase of NiSi at Ni/SiO_x interfaces towards thermodynamically stable antioxidation behavior. Remarkably, with this improved interfacial engineering, the oxidation of 80-nm-diameter Ni nanochain-SiO_x saturates after annealing at 550 °C in air for 12 h. Additional annealing at 550 °C in air for as long as 20 h (i.e., 32 h air annealing at >550 °C in total) has almost no further impact on the structural or optical properties of the coatings, the latter being very sensitive to any interfacial changes due to the localized surface plasmon resonances of the metal nanostructures. This phenomenon holds true for Ni nanoparticle diameter down to 40 nm in Ni-SiO_x system, where the optical response remains stable for 53 h at 550 °C in air. The oxidation vs. time curve also shows saturation behavior deviating from the kinetic Deal-Grove oxidation model. These results strongly suggest a promising approach to *thermodynamically stable*, anti-oxidation Ni/SiO_x cermet absorbers via interfacial engineering. © *2016 AIP Publishing LLC*. [http://dx.doi.org/10.1063/1.4945035]

I. INTRODUCTION

Cermet selective solar thermal absorbers,[1,2] usually consisting of metal nanoparticles (NPs) embedded in surrounding dielectric matrices,[1–3] are widely used in concentrated solar power (CSP) systems to maximize the optical absorption of sunlight while minimizing thermal emittance losses. However, there are two significant limitations in their fabrication and operation. First, cermet coatings usually require vacuum deposition for thickness control in order to optimize the optical properties, thereby increasing the fabrication cost. Second, metal particles, especially NPs, react with oxygen very quickly due to their large specific surface areas.[4] To prevent the oxidation of metal nanostructure at high working temperatures, currently, the CSP receiver has to be operated in vacuum. This increases the cost of system maintenance. In fact, the vacuum breaching failure becomes a major reliability problem of the CSP systems. All these issues call for a low-cost fabrication method to synthesize high-temperature, atmospherically stable cermet selective solar thermal absorbers for vacuum-free CSP systems.

Our previous results[5] demonstrated a solution-chemical method to fabricate Ni nanochain-SiO_x ($x < 2$) selective solar absorbers without vacuum deposition. These coatings showed oxidation-resistant behavior at 450–600 °C in air for several hours, as well as a high solar absorptance of 90% and a low thermal emittance of ~18% at 300 °C. We also found that the SiO_x ($x \sim 1.5$) matrix was more beneficial for antioxidation behavior than stoichiometric SiO_2 matrix, indicating that the antioxidation mechanism is closely related to the excess Si in the matrix. In Ref. 5, we preliminarily proposed a mechanism that the dissociation of Si-O cage-like structures/networks at high temperatures and the excess Si in the

a)Author to whom correspondence should be addressed. Electronic mail: Jifeng.Liu@dartmouth.edu. Tel.: +1-603-646-9885. Fax: +1-603-646-8778.

SiO_x ($x < 2$) matrix enabled or facilitated Ni silicide formation at the Ni/SiO_x interfaces, contributing to the excellent anti-oxidation behavior. The interfacial metal silicide formation kinetically slows down the oxidation process of metals due to its high thermal stability and much better resistance to oxidation.[6,7] However, it was unclear whether such a mechanism can be further extended *beyond kinetically* reduced oxidation rate and towards *thermodynamically* stable, long-term anti-oxidation behavior. In addition, notable silicide formation was observed only after annealing in air.[5] If interfacial silicides with high thermal stability can be formed before operating in air, the antioxidation behavior could be further enhanced.

In this work, we demonstrate that pre-operation annealing of Ni nanochain-SiO_x cermets at 900 °C in N_2 forms thermodynamically stable orthorhombic phase of NiSi at the Ni/SiO_x interfaces, in contrast to the less stable hexagonal NiSi phase obtained at a lower pre-operation annealing temperature of 750 °C followed by air annealing at 450–600 °C. Remarkably, with this improved interfacial engineering, *self-terminated oxidation* is observed in this system upon long-term annealing in air at 550 °C, as indicated by the stabilized optical reflectance spectra and the saturation of oxidation vs. time curve deviating from the kinetic Deal-Grove oxidation model. These results suggest the feasibility of *thermodynamically stable*, anti-oxidizing Ni-SiO_x cermet solar absorbers based on interfacial engineering. To the authors' knowledge, such self-terminated oxidation has only been reported in isolated Ag NPs due to the increase in surface/interface energy upon oxidation,[8] and it has not been observed in or applied to cermet solar selective absorbers before. Such mechanisms can potentially be optimized to achieve long-term, high-temperature, atmospheric-stable selective solar absorbers for advanced CSP systems.

II. EXPERIMENTAL

The detailed procedure of fabricating Ni nanochain-SiO_x ($x < 2$) selective solar thermal absorbers has already been discussed in Refs. 5 and 9. The average diameters of the Ni NPs used in this study range from 40 to 80 nm, controlled by the fabrication recipe. Ni NP chains mixed with hydrogen silsesquioxane (HSQ) precursors were spin-coated or drop-coated on Si and stainless steel (SS) substrates. The thickness of the coating is controlled to be ~1 μm for desirable solar-selective optical properties. HSQ consists of Si-H bonds, Si-O networks, and Si-O cage-like structures with a Si:O ratio of 1:1.5.[5,10] Therefore, the excess Si from HSQ (compared to stoichiometric SiO_2) reacts with Ni NPs to form interfacial silicides upon annealing, leading to a better anti-oxidation performance. In our previous research, however, significant interfacial silicide formation was not observed until *after* annealing in air. If interfacial silicides with high thermal stability can be formed *before* operating in air, we would expect a stronger antioxidation performance. To achieve this goal, in this work, a higher pre-operation annealing temperature of 900–920 °C in N_2 was applied, compared to 750 °C in our previous work. This method not only further enhances chemical bonding dissociation of the HSQ matrix but also generates more Si-rich, thermodynamically stable Ni silicide phases (e.g., orthorhombic NiSi phase) that favor anti-oxidation behavior at high-temperatures. Indeed, temperature-dependent phase transitions between Ni silicides in the form of continuous thin films have been reported in earlier studies,[11,12] which can be extended to cermet systems and engineered for improved anti-oxidation properties. Furthermore, to understand the mechanisms of anti-oxidation behavior, some samples were then annealed in air from 450 °C to 550 °C for different time durations up to 53 h. This temperature range is the most relevant to the parabolic trough CSP receivers.[1,2]

In order to analyze the interfacial silicide formation, X-ray photoelectron spectroscopy (XPS) was applied to characterize the chemical bonds, and transmission electron microscopy (TEM) was used to investigate interface structures and silicide phases via selected area electron diffraction (SAED). Optical reflectance spectroscopy incorporating an integrating sphere was not only applied to characterize the optical performance but also used as an extremely sensitive probe to reveal any interfacial changes because of the high sensitivity of localized surface plasmon resonances (LSPRs) to the surrounding.[13]

III. RESULTS AND DISCUSSION

A. Chemical bonding analysis

As mentioned earlier, the formation of interfacial silicides was not obvious after pre-operation annealing at 750 °C in N_2.[5] The XPS data only showed a slight shift in Ni 2p peaks compared to pure Ni, while the corresponding signal of Ni-Si bonds was very weak for the Si 2p peaks. It would be much more desirable to form stable interfacial silicides directly upon pre-operation annealing in order to enhance the antioxidation behavior. When increasing the pre-operation annealing temperature from 750 to 900 °C in this work, we found that the interfacial silicide formation is significantly enhanced. Fig. 1 shows the Si 2p spectra of the Ni-SiO_x ($x < 2$) sample annealed at 900 and 750 °C in N_2, respectively. A peak around 99.4 eV shown in the 900 °C annealed sample differentiates itself from the 750 °C annealed one. According to Si $2p_{3/2}$ peaks' locations in Ni

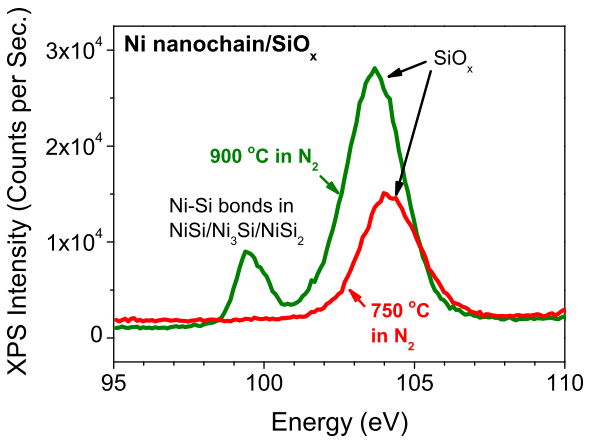

FIG. 1. XPS spectra (Si 2p) of Ni nanochain-SiO_x ($x < 2$) cermet coating on Si wafer annealed in N_2 at 750 °C (red) and 900 °C (green) for 30 min, respectively.

silicides,[14,15] this additional peak could be NiSi and/or Ni_3Si (both at ~99.4 eV). Since the peak is relatively broad, it could also incorporate $NiSi_2$ (99.6 eV) within the error range. Therefore, the XPS results indicate that the Ni silicide formation at the Ni/SiO_x interface is significantly enhanced upon 900 °C annealing in N_2 compared to that at 750 °C. Note that XPS only probes ~10 nm beneath the sample surface, while the film is 1 μm thick. Therefore, it cannot penetrate through the entire thin film and see the coating/substrate interface, i.e., we can exclude the substrate's impact.

There could be three possibilities to explain the difference. First, a higher annealing temperature (900 °C) provides a greater thermodynamic driving force towards silicide phase transitions. Indeed, Refs. 11, 16, and 17 discussed the phase transition from Ni_2Si (250–300 °C) to NiSi (320–550 °C) to $NiSi_2$ (>750 °C) in solid phase reactions between Ni thin films and Si substrates. Obviously, the annealing temperature is important to the selectivity of silicide phases. However, note that the respective silicide formation temperature may depend on the synthesis method, and in our case, the silicide formation temperature seems to be much higher than those for the thin film reactions because the reactant is SiO_x ($x \sim 1.5$) instead of Si. The second reason might be that the interfacial diffusion is enhanced at a higher temperature to kinetically facilitate silicide formation. It has been reported[16,18,19] that Ni silicide phase transformations are dominated by the diffusion of Ni. Finally, more Si-O cages/networks and Si-H bonds in the matrix tend to dissociate at a higher temperature. This is supported by the shift of Si 2p peak in SiO_x to lower energy upon annealing at 900 °C compared to 750 °C. By providing more excess Si upon HSQ matrix dissociation, the chemical equilibrium is driven toward the direction of Ni silicide formation. These three factors may contribute to this consequence jointly. Based on the explanation above, we can conclude that the Ni silicide formation at the Ni/SiO_x interface is strongly enhanced at elevated pre-operation annealing temperatures.

B. TEM analysis

In this section, we further confirm the interfacial formation of Ni silicides for the samples annealed at 900 °C in N_2 using TEM analysis.

In order to calibrate the electron diffraction patterns for phase identification, standard silver NPs (50 nm) were used as a reference. Under the same camera length (L) with the same voltage, $L\lambda$ is a constant, where λ is the electron wavelength determined by the applied voltage. It is well known that $Rd = L\lambda$, where R is the distance from the diffraction point to the center point (or the radius of the diffraction ring) and d is the inter-planar spacing in real lattices. Thus, the SAED pattern of unknown phases can be identified by matching the measured interplanar spacings to the Powder Diffraction File database using the calibrated $L\lambda$.

Figs. 2(a)–2(d) show the TEM images and SAED patterns of Ni-SiO_x ($x < 2$) samples annealed in N_2 at 900 °C. For comparison, Figs. 2(e) and 2(f), respectively, show the TEM image and the SAED pattern of Ni-SiO_x ($x < 2$) samples annealed in N_2 at 750 °C followed by air annealing at 450 °C for 4 h and 600 °C for 40 min. From Figs. 2(a) and 2(b), we can clearly see core/shell structures. To identify the phases of these structures, SAED patterns (Figs. 2(c) and 2(d)) show diffraction spots from these nanostructures. For smaller particles in Fig. 2(a) (~40 nm diameter), most diffraction points are from the Ni core since it is thin enough for the electron beam to penetrate through the entire structure. In contrast, for bigger particles in Fig. 2(b) (~80 nm diameter), we mostly see the diffraction spots from orthorhombic structured NiSi because the Ni core is too thick for the incident electrons to penetrate through. Considering a

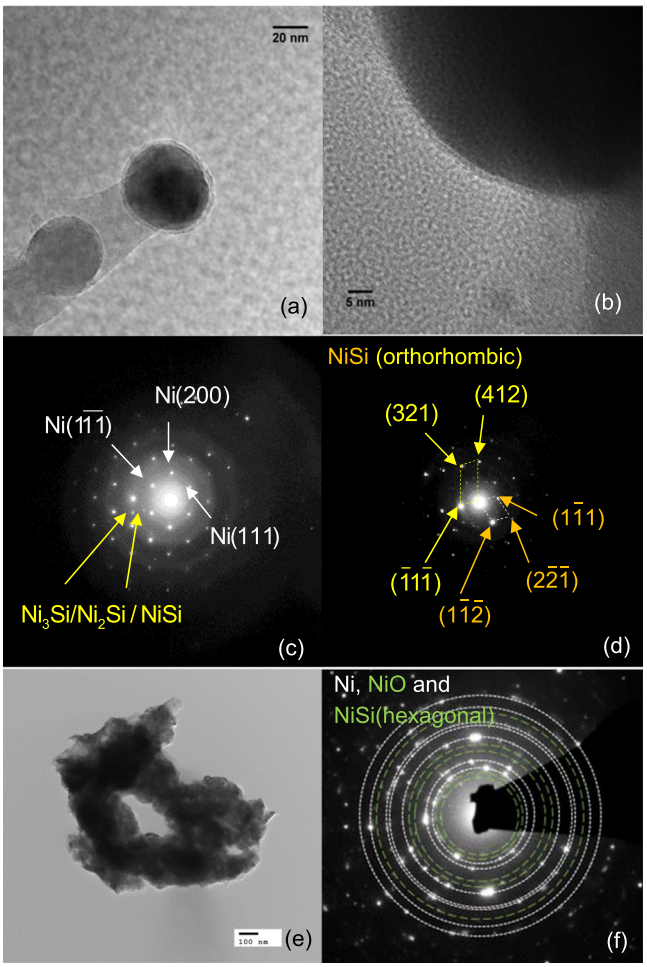

FIG. 2. TEM images of Ni/Ni silicide core/shell structures from the Ni-SiO_x ($x < 2$) cermet samples annealed in N_2 at 900 °C: (a) 40 nm diameter, and (b) 80 nm diameter. The SAED patterns in (c) and (d) correspond to (a) and (b), respectively. The diffraction spots in (c) correspond to Ni and Ni silicide(s), where the silicide phase could be NiSi, Ni_2Si, or Ni_3Si. The SAED pattern in (d) is identified to be orthorhombic structured NiSi. The Miller indices of the diffraction spots from two NiSi grains are labelled in yellow and orange, respectively. Their (1$\bar{1}$1) planes are parallel to one another. By comparison, (e) and (f), respectively, show the TEM image and SAED pattern of Ni-SiO_x ($x < 2$) cermet samples annealed in N_2 at a lower temperature of 750 °C, followed by air annealing at 450 °C for 4 h and 600 °C for 40 min. In (f), the white dashed circles correspond to the diffraction spots from Ni. From the inner to the outer circles, the Miller indices are {111}, {200}, {220}, {311}, {222}, {400}, and {331} + {422}, respectively. The green circles correspond to the diffraction spots from NiO and the metastable, *hexagonal* structured NiSi. The Miller indices from inner to outer circles are: NiSi{101} + NiO{111}, NiSi{102}, NiSi{103} + NiO{220}, NiSi{201} + {004}, and NiO{442}. The scale bars in (a), (b), and (e) are 20, 5, and 100 nm, respectively.

spherical model, most of the SAED data should come from the relatively thin peripheral region, which is the shell and nearby region in this case. Hence, these data directly confirm the interfacial formation of a Ni silicide shell around the Ni core. In Fig. 2(d), the Miller indices of the diffraction spots from two orthorhombic structured NiSi grains are labelled in yellow and orange, respectively. Their $(1\bar{1}1)$ planes are parallel to one another. Note that NiSi has two crystal structures: the thermodynamically stable orthorhombic phase[20,21] and the metastable hexagonal phase.[22] Therefore, the formation of orthorhombic structured NiSi after annealing at 900 °C in N_2 is more beneficial for the thermal stability.

By comparison, for the Ni-SiO_x sample annealed in N_2 at 750 °C, silicide formation was not observed until after further air annealing at 450 °C for 4 h and 600 °C for 40 min. After air annealing, it is hard to obtain isolated Ni NPs due to the inherent nanochain structure[5,9] and enhanced adhesion between the Ni NPs and the SiO_x matrix. Fig. 2(e) shows a Ni NP loop embedded in SiO_x, and the corresponding SAED pattern in Fig. 2(f) shows diffraction spots from Ni, NiO, and *hexagonal* structured NiSi (metastable). The diffraction spots from Ni are outlined by the white dashed circles, while those from NiO and hexagonal structured NiSi are outlined by the green ones. The corresponding Miller indices are given in the figure caption. Note that in this case only the metastable NiSi (hexagonal structure) is formed, in contrast to the thermodynamically stable, orthorhombic structured NiSi directly obtained upon pre-operation annealing at 900 °C in N_2. This result confirms that increasing the pre-operation annealing temperature from 750 to 900 °C strongly enhances the formation of stable NiSi at the Ni/SiO_x interfaces, thereby improving the thermal stability of the Ni-SiO_x cermet system. As will be shown in Sec. III C, this interfacial engineering could lead to a thermodynamically stable state, where the oxidation of the NPs can spontaneously slow down and even terminate eventually. This is because further oxidation would induce such a large increase in the interfacial energy that it overwhelms the Gibbs free energy reduction of the oxidation reaction itself, thereby ending the oxidation process.

C. Towards thermodynamically stable, long-term anti-oxidation behavior

1. Saturation behavior in oxidation vs. time curve upon air annealing

In Ref. 5, we have studied the oxidation of Ni-SiO_x cermets for up to 2 h at 450–675 °C. The extent of oxidation was characterized by the X-ray diffraction (XRD) peak intensity ratios of NiO(200) to Ni(111) since NiO was identified to be completely crystalline (also confirmed by the diffraction spots from NiO in Fig. 2(f)). Within the annealing period of 2 h, the oxidation vs. time curve follows the Deal-Grove model for annealing temperatures <600 °C. This model considers O_2 diffusion as the dominating mechanism for long-term oxidation and predicts that the extent of oxidation is proportional to the square root of oxidation time. Here, we apply similar characterization methods to the samples pre-annealed at 900 °C in N_2 with strongly enhanced interfacial silicide formation, as discussed earlier, and we significantly increase the air annealing time to >30 h in order to investigate the long-term antioxidation behavior.

Fig. 3(a) shows the XRD data for the Ni-SiO_x samples annealed in air at 450 °C for 4 h followed by 550 °C for 12 h and 32 h, respectively. The XRD pattern of the SS substrate is also shown as a reference. The average diameter of the Ni NPs is 80 nm. As discussed in Ref. 5, the 450 °C annealing had induced negligible oxidation, so nearly all the NiO were grown during the 550 °C air annealing. Remarkably, the XRD data for 12 h and 32 h annealing are almost identical, indicating nearly no further oxidation after 12 h at 550 °C. The identical widths of the Ni XRD peaks also indicate that the size of the Ni nanocrystals remains the same. This is also confirmed by the nearly identical reflectance spectra, as will be discussed in Sec. III C 2. Fig. 3(b) further summarizes the Ni(200) to Ni(111) XRD peak ratio for the Ni-SiO_x system annealed in air at 550 °C for up to 32 h. Clearly, the classical Deal-Grove kinetic oxidation model far overestimates the long-term oxidation compared to the experimental results. By comparison, the solid green curve shows another fitting

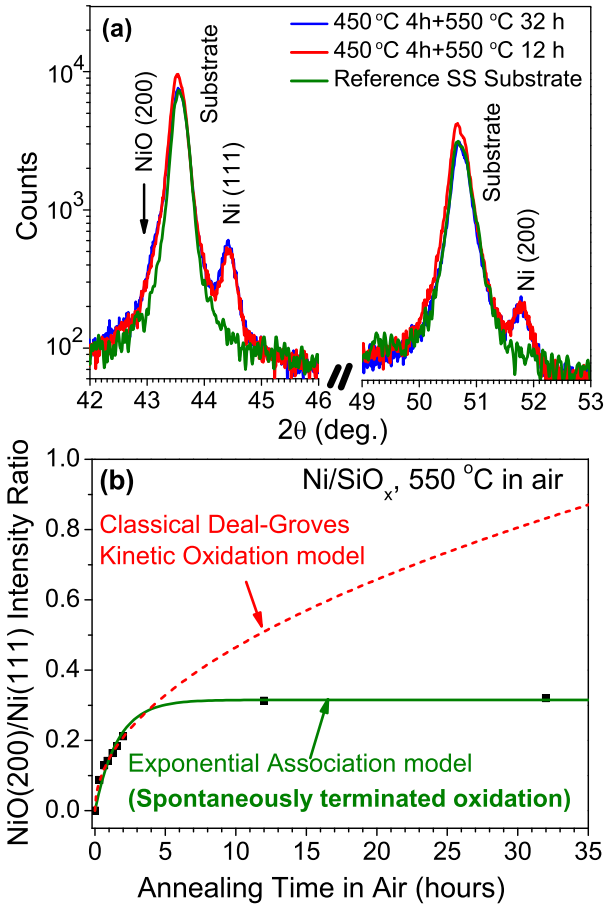

FIG. 3. (a) XRD data of the Ni-SiO_x ($x < 2$) samples annealed in air at 450 °C for 4 h, followed 12 h and 32 h air annealing at 550 °C, respectively. The XRD pattern of the stainless steel (SS) substrate is also shown as a reference. The average diameter of the Ni NPs is 80 nm. (b) NiO(200)/Ni(111) XRD peak ratio vs. annealing time in Ni-SiO_x ($x < 2$) system at 550 °C in air. The dashed lines show the fitting curves using classical Deal-Grove oxidation model. The solid line shows a fitting curve using phenomenological exponential association model, indicating an oxidation saturation after ~5 h. Obviously, the latter fits the experimental data much better than the Deal-Grove kinetic oxidation model, strongly suggesting self-terminated oxidation in Ni-SiO_x cermet system.

using an phenomenological exponential association model $r_{NiO/Ni} = A(1 - e^{-t/\tau})$ to capture the oxidation saturation after long-time annealing and the reaction limited linear oxidation as $t \sim 0$.[5] Here, $r_{NiO/Ni}$ is the XRD peak intensity ratio of NiO(200) to Ni(111), while A and τ are fitting parameters. Obviously, this fitting agrees very well with the experimental data. Therefore, Fig. 3 provides strong evidence that the oxidation process in Ni-SiO_x cannot only be retarded kinetically but also be spontaneously ***terminated*** via adequate interfacial engineering of Ni silicides, e.g., using pre-operation annealing at 900 °C to boost the formation of thermodynamically stable, orthorhombic structured NiSi at the Ni/SiO_x interface. It also demonstrates that the thermodynamically stable antioxidation mechanism can be achieved.

2. Evolution of reflectance spectra upon air annealing

The self-terminated oxidation upon long term air annealing is also confirmed by the reflectance spectra. Optical properties of the plasmonic Ni-SiO_x cermets are not only important for the application as solar selective absorbers but also a sensitive probe of any interfacial modifications since the LSPRs are significantly influenced by the interfacial environment.[13,23] Indeed, previous literature has demonstrated that a monolayer of surface oxide on silver NPs can induce a remarkable shift of the LSPR.[24] As an example for our case, Fig. 4(a) shows the theoretically simulated extinction spectrum of Ni nanochains in SiO_x with and without a 5 nm Ni_3Si shell. The response was calculated based on the optical parameters of Ni and Ni_3Si using finite element solutions of the Maxwell equations described in Refs. 5 and 9. The extinction factor in the vertical axis is defined as the optical extinction cross-section divided by the cross-section of the Ni NPs. It is directly proportional to the extinction coefficient at a given wavelength. The higher the extinction coefficient, the higher the spectral absorptance (α_λ). As shown in Fig. 4(a), even such a 5-nm thin Ni_3Si shell induces a notable red-shift of the optical extinction spectrum by ~500 nm, which would transfer to a red-shift of the spectral absorptance. Since the optical transmittance through the SS

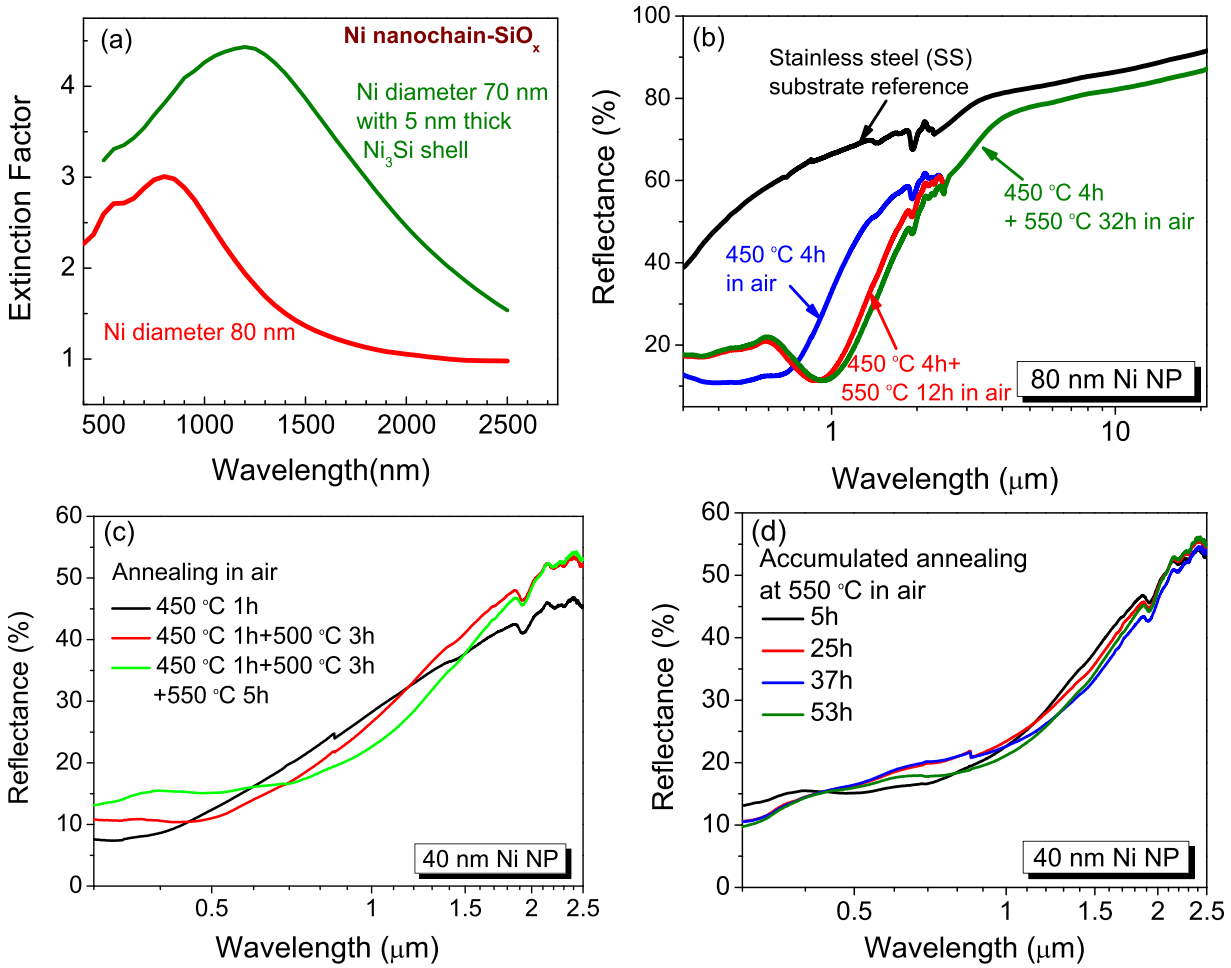

FIG. 4. (a) Theoretically calculated optical response of Ni nanochain-SiO_x ($x < 2$) with and without a 5 nm thick Ni_3Si shell using the methods in Refs. 5 and 9. The extinction factor refers to the extinction cross-section divided by the cross-section of the Ni NPs. It is proportional to the extinction coefficient.[5] (b) Experimentally measured reflectance spectra of Ni-SiO_x on SS substrate annealed at 450 °C for 4 h in air, followed by 12 h and 32 h air annealing at 550 °C, respectively. The average Ni NP diameter is 80 nm in this case. The reflectance spectra for 12 and 32 h annealing at 550 °C are almost identical, consistent with the XRD data in Fig. 3. The measured reflectance from the stainless steel (SS) substrate is also shown as a reference. (c) The reflectance spectra of Ni-SiO_x samples with 40 nm diameter Ni NPs annealed in air at 450–550 °C. Two red-shifts are observed when the annealing temperature is increased from 450 to 500 °C, and from 500 to 550 °C, respectively. (d) The reflectance spectra of Ni-SiO_x samples with 40 nm diameter Ni NPs annealed in air at 550 °C for 5–53 h. A similar stabilization of reflectance spectrum is observed after 5 h annealing. Further annealing up to 53 h has little impact on the reflectance spectrum.

substrate is 0, at each wavelength λ, the spectral absorptance α_λ and spectral emittance ε_λ are related to the reflectance $R(\lambda)$ by[1,2]

$$\alpha_\lambda = \varepsilon_\lambda = 1 - R_\lambda. \quad (1)$$

Therefore, the redshift in the optical extinction/spectral absorptance spectrum due to the interfacial modification would also induce a redshift in the reflectance spectrum. Conversely, changes in the optical reflectance spectra can also be applied to evaluate the interfacial oxidation process with high sensitivity.

Fig. 4(b) shows the reflectance spectra of the Ni-SiO_x sample on SS substrates after different stages of air annealing, the average Ni NP diameter being 80 nm. After annealing in air at the 450 °C for 4 h, the reflectance is ~10% in the wavelength regime of $\lambda = 300$–850 nm (UV, visible, and near-infrared (NIR)), and it starts to increase at $\lambda = 1\ \mu$m. After further annealing the sample at 550 °C for 12 h, the reflectance spectrum significantly red-shifted by ~0.4 μm. This is due to the enhanced silicides and NiO formation at the interface that influences the plasmonic response, consistent with the theoretical analysis in Fig. 4(a). Interestingly, further annealing at 550 °C for as long as 20 h (i.e., 32 h in total) has almost no more impact on the reflectance spectrum, indicating little interfacial changes upon extended air annealing. This observation agrees with the saturated oxidation demonstrated in Fig. 3. Similarly, for the Ni-SiO_x sample with 40 nm diameter Ni NPs, the reflectance is <10% at $\lambda = 300$–500 nm after annealing in air at 450 °C for 1 h, and it starts to increase at ~450 nm. The blue-shifted spectrum compared to that of the 80 nm diameter sample is due to the smaller Ni NP size and the corresponding blue-shift of the LSPR, consistent with our theoretical analysis in Ref. 9. After annealing at 500 °C for 3 h and 550 °C for 5 h, the spectrum red-shifted twice by ~0.1 μm and ~0.16 μm, respectively, again due to the enhanced interfacial reactions at higher temperatures. Fig. 4(d) further shows that the saturated oxidation behavior also holds for 40 nm diameter Ni NPs in SiO_x, where annealing in air at 550 °C for 5–53 h has almost no impact on the reflectance spectra. There is no deterioration in mechanical integrity, either. The results in Figs. 3 and 4 strongly suggest that the oxidation process terminates at a thermodynamically stable stage with adequate interfacial engineering. This thermodynamically stable anti-oxidation behavior indicates a promising prospect for Ni-SiO_x cermets to withstand long-term oxidation at high temperatures.

The overall solar absorptance α_{sol} and thermal emittance ε_{therm} can be derived from the reflectance spectra in Fig. 4(b) by

$$\alpha_{sol} = \frac{\int I_{sol,\lambda}\alpha_\lambda d\lambda}{\int I_{sol,\lambda} d\lambda} = \frac{\int I_{sol,\lambda}(1 - R_\lambda) d\lambda}{\int I_{sol,\lambda} d\lambda}, \quad (2a)$$

$$\varepsilon_{therm} = \frac{\int I_{black,\lambda}\varepsilon_\lambda d\lambda}{\int I_{black,\lambda} d\lambda}. \quad (2b)$$

Here, $I_{sol,\lambda}$ is the radiation intensity at wavelength λ in AM 1.5 solar spectrum, and the integration wavelength range is 0.25–2.5 μm. $I_{black,\lambda}$ is the black body radiation intensity at wavelength λ, and the integration wavelength range is 2.5–25 μm. $I_{black,\lambda}$ is often evaluated at 300 K for comparison.

According to Eq. (2), the α_{sol} after 4 h annealing at 450 °C in air is ~76.7% from Fig. 4(b) for 80 nm diameter Ni NPs. After further annealing at 550 °C in air for 12 and 32 h, α_{sol} increases to 79.2% and 79.5%, respectively. The increase is mainly due to the redshift of the spectrum, despite the increase in reflectance at shorter wavelengths. The 40 nm-diameter Ni NPs in Fig. 4(d) also demonstrate an α_{sol} of ~80%. The reflectance in the visible and near IR regime ($\lambda < 2\ \mu$m) can be further reduced by well-established antireflection coating techniques[1,2] in order to further increase α_{sol}. The overall thermal emittance is 20% for the sample with 80 nm-diameter Ni NPs annealed in air at 550 °C for 32 h. Fig. 4(b) also shows that the IR reflectance is mainly limited by the unpolished SS substrate itself (~80%, corresponding to 20% emittance). It is expected that the IR reflectance can be further increased and thermal emittance decreased by using an IR reflector coating.[1,2]

3. Mechanism of the self-terminated oxidation process in Ni-SiO_x cermets

As discussed in Secs. III C 1 and III C 2, the Ni-SiO_x demonstrates a self-terminated oxidation behavior in air at 550 °C. This is highly desirable for long-term, vacuum-free operations of these coatings. It is intriguing to investigate why such small NPs (40–80 nm in diameter) can resist oxidation so effectively. Since the oxidation vs. time curve deviates from the kinetic Deal-Grove model, such stability is most likely induced by the thermodynamic process. Due to the large specific surface area of the metal NPs, the surface/interface energy contributes significantly to the Gibbs free energy change ΔG. Oxidation process naturally forms new surfaces/interfaces. If the increase in surface/interface energies exceeds the Gibbs free energy reduction due to the oxidation reaction itself, the oxidation process will terminate and a *thermodynamically stable* system *against further oxidation* could be obtained.

Indeed, similar self-terminated oxidation has been reported in isolated Ag NPs larger than a critical radius (R_c),[8] where the high-temperature oxidation at 700 °C spontaneously terminates due to the increase in surface/interfacial energy with the oxide thickness. A thermodynamic model has been established by Bi *et al.*[8] to explain this phenomenon. The model employs a classical description of the curvature and surface effects, and yields the Gibbs free energy change upon oxidation

$$\Delta G = \Delta G_0 + Se^{-\frac{\delta}{d}} + \Delta G_s + \Delta G_c, \quad (3)$$

where ΔG_0, ΔG_s, and ΔG_c are the bulk, surface, and curvature contributions to the Gibbs free energy change upon oxidation, respectively. The term $Se^{-\frac{\delta}{d}}$ describes the interaction between the two interfaces on both sides of the oxide layer separated by its thickness d. As the surface and curvature

contributions depend on the interfacial energies γ_i and the radius of each shell layer R_i, ΔG is a strong function of particle size. Remarkably, the model further predicts that for large enough NPs the metal NP-oxide core-shell structure can be thermodynamically stable against further oxidation, featured by the presence of a minimum in the free energy change ΔG with respect to the oxide layer thickness. As schematically shown in Fig. 5(a), the Gibbs free energy initially decreases with the oxidation before it reaches this minimum; yet as the oxide layer grows, the corresponding increase in surface/interfacial energy eventually leads to an increase in the overall Gibbs free energy. Therefore, the oxidation spontaneously terminates at the ΔG minima. Theory also predicts that the minimum in ΔG only occurs when the radius of the NP falls within a certain range. If the particles are too small ($R < R_c$), they would be fully oxidized before reaching the ΔG minima (see Fig. 5(a)). If the particles are in micron-meter scale instead of nanoscale, the interfacial energy plays too little role to prevent further oxidation, and the material oxidation would be similar to their bulk counterparts.

In our case, the interfacial silicide formation provides more interfaces than the oxidation of Ag NPs, as schematically shown in Fig. 5(b). This further stresses the influence of interfacial energies upon oxidation. Considering that the antioxidation behavior is only observed in Ni-SiO_x and not Ni-Al_2O_3 system,[5] the interfacial silicide formation must have played an important role in modifying the interfacial energy. In particular, the formation of the thermodynamically stable, orthorhombic structured NiSi at the Ni/SiO_x upon pre-operation annealing at 900 °C is highly beneficial for the long-term thermal stability. Furthermore, as has been discussed in Ref. 5, Raman spectroscopy indicates a compressive strain in the silicide layers upon oxidation. Therefore, the increase in the interfacial energy and strain energies upon oxidation may have effectively induced a ΔG minimum in the oxidation process of Ni-SiO_x cermets. This theory also qualitatively explains why such phenomenon is not observed in conventional cermets based on Ni. In conventional cermets, the metal NPs typically have a diameter <10 nm,[1,2] too small to reach the critical radius R_c. Therefore, long-term antioxidation behavior has ***not*** been observed in conventional cermets. Our solution processed plasmonic metal NP cermets provide a unique opportunity in that the diameter of metal NPs is increased to 40–100 nm,

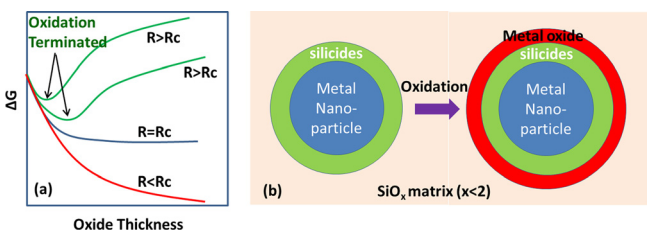

FIG. 5. (a) Schematics of the Gibbs free energy change (ΔG) vs. oxide thickness of metal NPs.[8] The ΔG curve shows a minimum when the radius (R) of the NP exceeds a critical radius R_c, indicating that the complete oxidation of NP is thermodynamically prohibited and the oxidation will terminate spontaneously at a certain stage.[8] (b) Schematic structures of the oxidation process in metal-SiO_x ($x < 2$) cermet system. A silicide layer is introduced by interfacial reaction between Ni and SiO_x in this case.

exceeding the critical radius R_c for thermodynamically stable antioxidation behavior. Further considering our experimental results on the self-terminated oxidation for 40 nm and 80 nm diameter Ni NPs in SiO_x in Figs. 3 and 4, we can estimate $5\,nm < R_c < 20\,nm$ in Ni-SiO_x system. Due to the lack of interfacial energy data in Ni-SiO_x system, we are unable to quantitatively evaluate R_c at termination theoretically. Experimental studies on smaller Ni NPs in SiO_x are currently limited by the clustering of Ni NPs. The studies on the critical radius R_c for self-terminated oxidation process in Ni-SiO_x system will be continued in our future work.

IV. CONCLUSIONS

In this work, we have investigated the mechanism for high-performance anti-oxidation Ni nanochain-SiO_x ($x < 2$) cermet solar selective absorbers towards long-term, air-stable operations at ≥550 °C. We demonstrate that high-temperature (>900 °C), pre-operation annealing in N_2 enhances interfacial silicide formation, as confirmed by XPS and TEM analyses. Remarkably, the oxidation of these interfacially engineered Ni/silicide core/shell structures shows a saturation behavior with the increase of annealing time in air for Ni NP diameters of 40–80 nm, notably deviating from the kinetic Deal-Grove oxidation model. This self-terminated oxidation is also confirmed by the nearly identical optical reflectance spectra for the Ni-SiO_x cermet samples with 80 nm diameter Ni NPs annealed between 12 and 32 h at 550 °C in air, which is very sensitive to any interfacial changes due to the LSPRs of the metal nanostructures. Similar phenomenon has been observed for 40 nm diameter Ni NPs in Ni-SiO_x system between 5 and 53 h annealing in air at 550 °C. We attribute the excellent anti-oxidation behavior to thermodynamic mechanisms involving significant contributions from the interfacial energies of the metal/silicide core-shell structures upon oxidation, similar to those in the self-terminated oxidation of Ag NPs.[8] Due to the increase in the interfacial energy and strain energy of the interfacial silicide layer upon oxide growth, ΔG is minimized at a certain oxide thickness for NPs exceeding a critical size. Further oxidation would induce a large increase in the interfacial/strain energy that exceeds the Gibbs free energy reduction of the oxidation reaction itself, thereby thermodynamically prohibited. This leads us to the feasibility of thermodynamically stable, anti-oxidation cermet solar selective absorbers for long-term antioxidation operations at high temperatures. In addition, the optical performance has no deterioration after long-term thermal annealing at 550 °C in air for >40 h. Overall, this interfacially engineered Ni-SiO_x cermet solar selective absorber, incorporating thermodynamically stabilized Ni NPs against high-temperature, long-term oxidation, has a great potential to meet the CSP receiver's anti-oxidation demands for air-stable operations in the future.

ACKNOWLEDGMENTS

Part of this work had previously been supported by the National Science Foundation (NSF) Small Business Innovation Research (SBIR) Program under Contract No. 1315245 via the subcontract from Norwich Technologies,

Inc. Currently, the work was supported by the Department of Energy, Office of Energy Efficiency and Renewable Energy (EERE), under Award No. DE-EE0007112. We would also like to thank Dr. Charles P. Daghlian at Dartmouth College for his help with the transmission electron microscopy.

[1]J. A. Duffie and W. A. Beckman, *Solar Engineering of Thermal Processes*, 3rd ed. (John Wiley & Sons, 2006,).
[2]C. E. Kennedy, *Review of Mid-to High Temperature Solar Selective Absorber Materials* (National Renewable Energy Laboratory (NREL) report, Washington, DC, 2002).
[3]C. M. Lampert, Sol. Energy Mater. **1**, 319 (1979).
[4]K. Park, D. Lee, A. Rai, D. Mukherjee, and M. R. Zachariah, J. Phys. Chem. B **109**, 7290 (2005).
[5]X. B. Yu, X. X. Wang, Q. L. Zhang, J. C. Li, and J. F. Liu, J. Appl. Phys. **116**, 073508 (2014).
[6]W. J. Strydom, J. C. Lombaard, and R. Pretorius, Thin Solid Films **131**, 215 (1985).
[7]J. P. Gambino and E. G. Colgan, Mater. Chem. Phys. **52**, 99 (1998).
[8]H. J. Bi, W. P. Cai, C. X. Kan, L. D. Zhang, D. Martin, and F. Träger, J. Appl. Phys. **92**, 7491 (2002).
[9]X. X. Wang, H. F. Li, X. B. Yu, X. L. Shi, and J. F. Liu, Appl. Phys. Lett. **101**, 203109 (2012).
[10]C. C. Yang and W. C. Chen, J. Mater. Chem. **12**, 1138 (2002).
[11]J. Foggiato, W. S. Yoo, M. Ouaknine, T. Murakami, and T. Fukada, Mater. Sci. Eng., B **114–115**, 56 (2004).
[12]M. Tinani, A. Mueller, Y. Gao, E. A. Irene, Y. Z. Hu, and S. P. Tay, J. Vac. Sci. Technol., B **19**, 376 (2001).
[13]H. Raether, *Surface Plasmon on Smooth and Rough Surface and Gratings* (Springer-Verlag, Berlin, 1986).
[14]Y. Cao, L. Nyborg, and U. Jelvestam, Surf. Interface Anal. **41**, 471 (2009).
[15]M. A. Peck and M. A. Langell, Chem. Mater. **24**, 4483 (2012).
[16]A. Julies, D. Knoesen, R. Pretorius, and D. Adams, Thin Solid Films **347**, 201 (1999).
[17]D. Ma, D. Z. Chi, M. E. Loomans, W. D. Wang, A. S. W. Wong, and S. J. Chua, Acta Mater. **54**, 4905 (2006).
[18]G. Utlu, N. Artunc, S. Budak, and S. Tari, Appl. Surf. Sci. **256**, 5069 (2010).
[19]F. F. Zhao, J. Z. Zheng, Z. X. Shen, T. Osipowicz, W. Z. Gao, and L. H. Chan, Microelectron. Eng. **71**, 104 (2004).
[20]F. d'Heurle, C. S. Petersson, J. E. E. Baglin, S. J. La Placa, and C. Y. Wong, J. Appl. Phys. **55**, 4208 (1984).
[21]J. Y. Dai, D. Mangelinck, and S. K. Lahiri, Appl. Phys. Lett. **75**, 2214 (1999).
[22]D. Connétable and O. Thomas, Phys. Rev. B **81**, 075213 (2010).
[23]J. A. Schuller, E. Barnard, W. S. Cai, Y. C. Jun, J. White, and M. L. Brongersma, Nat. Mater. **9**, 193 (2010).
[24]A. Kuzma, M. Weis, S. Flickyngerova, J. Jakabovic, A. Satka, E. Dobrocka, J. Chlpik, J. Cirak, M. Donoval, P. Telek, F. Uherek, and D. Donoval, J. Appl. Phys. **112**, 103531 (2012).